Size-Selective Electrodeposition of Mesoscale Metal Particles in the Uncoupled Limit

H. Liu and R. M. Penner*

Institute for Surface and Interface Science and Department of Chemistry, University of California, Irvine, Irvine, California 92679-2025

Received: May 15, 2000; In Final Form: July 10, 2000

In principle, metal particles can be electrodeposited on electrode surfaces under conditions where individual metal particles grow independently of neighboring particles on the electrode surface, and the growth rate for every particle on the surface is the same. In this "uncoupled limit", extremely narrow particle size distributions will be attainable. We describe the conditions of nucleation density and electrodeposition duration and rate for which this uncoupled growth regime can be obtained. When these growth conditions are implemented to grow silver and gold mesoscale particles on graphite electrode surfaces, narrow (RSD_{dia} < 10%) particle size distributions are obtained for particles with mean diameters in the range from 50 nm to 2.0 μm.

I. Introduction

Electrochemistry provides a means by which virtually any metal can be deposited at a precisely known coverage onto a conductive surface from an ionic solution. In this sense, electrochemistry is powerful and versatile. On the other hand, it has not been possible to directly deposit dimensionally uniform[1] metal structures (e.g., metal particles) on planar electrode surfaces: Mesoscale[2] metal particles have been obtained by electrochemical deposition; however, with two important exceptions,[3] the relative standard deviation of the particle diameter (RSD_{dia}) has been 20−50%.[4−6] Equally problematic is the tendency for the dimensional uniformity of electrodeposited structures to degrade as these structures increase in size beyond 100 Å.[4−6] The template synthesis method pioneered by the research groups of Martin,[7,8] Moskovits,[9] and Searson[10−12] provides one elegant and general solution to this problem. We have been seeking to develop "templateless" electrochemical routes to dimensionally uniform metal structures analogous to those based on physical vapor deposition (cf. refs 13−15). This development process must proceed from an understanding of the factors that contribute to particle size dispersion in electrochemical nanoparticle growth.

We are beginning to understand some of these factors. Recent Brownian dynamics simulations of diffusion-controlled metal particle growth have demonstrated that diffusional interparticle coupling provides a mechanism for the development of size dispersion on surfaces where nucleation is spatially random.[16] In these simulations, both absolute and relative measures of the particle size polydispersity increased as a function of deposition time for ensembles of metal nanoparticles even though these particles nucleated instantaneously, and grew at the diffusion-controlled rate. Experimentally, the Volmer−Weber growth of metal nanoparticles has been investigated for both silver[5] and platinum[4] on graphite surfaces. The rate at which particle size dispersion develops in these experiments is consistent with the results of the Brownian dynamics simulations.[16] We conclude that, in cases where particles nucleate instantaneously, "divergent growth" is caused by interparticle diffusional coupling.

* To whom correspondence should be addressed. E-mail: rmpenner@uci.edu.

If metal particles can be electrodeposited in an uncoupled mode—that is, under conditions where each particle grows at a rate that is independent of the number and proximity of neighboring particles on the surface—then the rate laws describing the growth of these particles will be identical to those which apply to the growth of colloid particles in solution. In that case, the path to improved size dispersion was mapped out my LaMer,[17] Reiss,[18] and others[19,20] 40 years ago. The key requirement is that the nucleation of particles be instantaneous. Beyond this, one wishes to encourage growth at diffusion control since the particle size distribution created by nucleation will narrow as a function of time as small particles "catch up to" larger particles in this distribution. If, instead, the particle growth reaction is kinetically controlled, distribution narrowing does not occur.[18] Rather the standard deviation of the size distribution remains constant as the mean particle diameter increases with deposition time. A key point is that, in the uncoupled regime, neither kinetically controlled nor diffusion-controlled growth leads to coursening, as normally seen in the growth by electrodeposition of particles. Williams and co-workers[21−23] have shown that the conclusions of LaMer and Reiss extend to the growth of particles on surfaces by physical vapor deposition. Thus, a clear motivation exists for understanding how to achieve uncoupled growth in an electrodeposition experiment.

In this paper we delineate the conditions of nucleation density, growth rate, and growth duration required for the uncoupled growth of metal particles on electrode surfaces. Using parameters within this "uncoupled domain", we demonstrate that uncoupled growth can be experimentally realized for the electrodeposition of silver and gold nano- and microparticles on graphite surfaces. The metal particle dispersions thereby obtained exhibit the highest degree of size monodispersity so far seen in an electrodeposition experiment.

II. Experimental Methods

II.A. Silver and Gold Electrodeposition. The electrodeposition of silver and gold particles was carried out in a glass, one-compartment, three-electrode cell. The silver plating solution contained 1.0 mM $AgClO_4$ (Alfa Aesar, 99.9%) with a supporting electrolyte of 0.1 M $LiClO_4$ (Aldrich, 99.99%) in acetonitrile (Burdick & Jackson, ultrapure). The gold plating

10.1021/jp0017902 CCC: $19.00 © 2000 American Chemical Society
Published on Web 09/08/2000

SCHEME 1: Spatial Relationship of Depletion Layers for the Uncoupled and Coupled Electrodeposition of Particles on an Electrode Surface

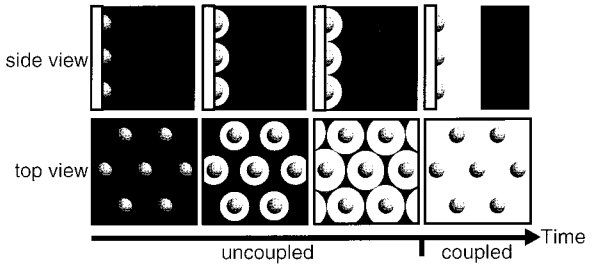

solution was 1.0 mM $AuCl_3$ (Aldrich, 99.99+%) and 0.1 M NaCl (Aldrich, 99+%) in water (Nanopure, $\rho > 18$ MΩ). These solutions were thoroughly sparged with N_2 before each experiment. The basal plane surface of a highly oriented pyrolytic graphite (HOPG) crystal was cleaved using Scotch tape immediately prior to use. Silver and gold particles were deposited using a double pulse experiment in which a 5.0 ms nucleation pulse was followed by a much longer growth pulse. For silver particle deposition, the 5 ms nucleation pulse involved the application of −500 mV vs Ag^0/Ag^+; for gold electrodeposition, the 5 ms pulse had an amplitude of 0.2 V vs SCE. The second, or growth, pulse was potentiostatic. Potentiostat and amperometric pulses were applied using an EG&G model 273 potentiostat/galvannostat. Following deposition, the graphite working electrode was removed from the plating solution and rinsed with pure acetonitrile.

II.B. Microscopy. Freshly rinsed samples were placed in a desiccator and stored overnight prior to examination. All scanning electron microscopy (SEM) measurements were conducted using a Philips model XL-30FEG at an accelerating voltage of 10 keV. NIH SXM 1.61 software was used to extract the particle diameter and areal densities from thresholded SEM images.

III. Results and Discussion

III.A. Strategies for Achieving Uncoupled Growth. For particles to grow independently of one another on an electrode surface, the depletion layers for adjacent particles must not coalesce during deposition. In other words, the deposition time, t_{dep}, must be less than the time at which depletion layers for neighboring particles coalesce, t_c (see Scheme 1). An expression for t_c can be derived for a potentiostatic experiment as follows. At the surface of a hemispherical metal particle, the concentration of a reactant ion as a function of radial distance, $C(r)$, rapidly reaches a steady state given by[24]

$$C(r) = C^* - \frac{(C^* - C_o)r_o}{r} \qquad (1)$$

where C^* is the concentration of metal ion in the bulk of the solution, C_o the concentration at r_o (the surface of the microelectrode). The value of C_o is in the range from 0 to C^* depending on the deposition overpotential that is selected, and on the kinetic facility of the deposition reaction. Let us define the "edge" of the depletion layer, r_d, as the radius at which $C(r)$ is $0.9C^*$. An equation for r_d can then be derived from eq 1:

$$r_d = \frac{(C^* - C_o)r_o}{0.1C^*} \qquad (2)$$

$C(r)/C^*$ is plotted as a function of r in Figure 1a. A key point,

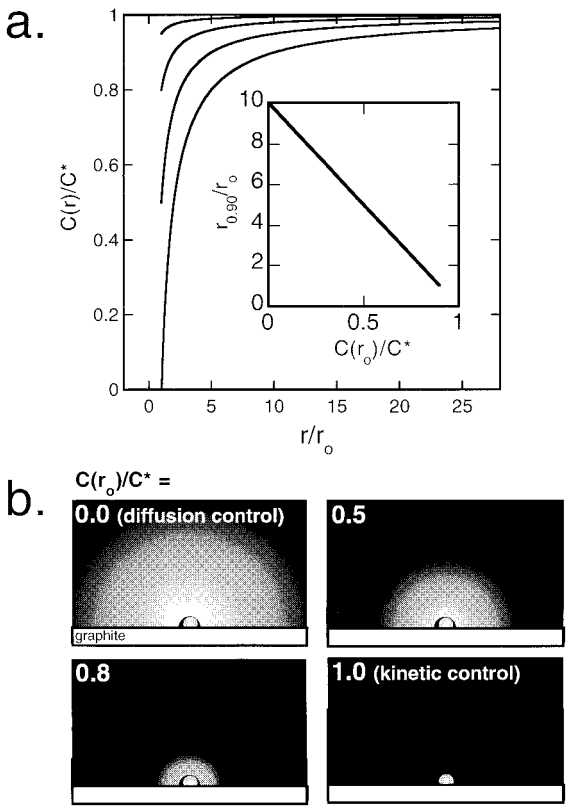

Figure 1. (a) Calculation of the steady-state, dimensionless concentration of metal ion, $C(r)/C^*$, as a function of the distance, r, from a hemispherical metal particle layer of radius r_o using eq 4. $C(r)/C^*$ is plotted for four values of the surface concentration, C_o/C^*, as indicated. (b) Schematic representation of the depletion layer near a growing metal particle for four different values of C_o/C^*, as indicated.

as shown schematically in Figure 1b, is that the thickness of the depletion layer (shown in gray) collapses from $r_d/r_o = 10$ to $r_d/r_o = 1$ as C_o/C^* is increased from 0 (corresponding to diffusion control) to 1. Thus, C_o (and hence the reaction rate) provides a straightforward means by which the diffusion-mediated interaction of adjacent metal hemispheres can be forestalled. In the limit of $C_o = C^*$ (corresponding to kinetic control of the reaction rate), no depletion layer exists and the interparticle diffusional coupling is eliminated.

To calculate $r_d(t)$ using eq 2, an expression for the time dependence of r_o is needed. Two scenarios of interest are growth at diffusion control in which case $r_o(t)$ is given by[25,26]

$$r_o(r) = \left[\frac{2DC^*(1 - C_o/C^*)Mt}{\rho}\right]^{1/2} \qquad (3)$$

where for silver the following materials parameters obtain: $M_{Ag} = 107.87$ g/mol, $D_{Ag^+} = 1.35 \times 10^{-5}$ cm^2/s, $\rho_{Ag} = 10.5$ g/cm^3. A second possibility is that growth occurs under conditions of constant total current, i_{dep}, in which case $r_o(t)$ is given by

$$r_o(t) = \left[\frac{3}{2}\frac{i_{dep}tM}{z\pi\rho FN}\right]^{1/3} \qquad (4)$$

where z is the number of electrons transferred per metal ion (equiv/mol), F is the Faraday constant (96 485 C equiv^{-1}), and N is the nucleation density (cm^{-2}).

An expression for the overlap time, t_c, can be obtained from either eq 3 or eq 4 and for any geometric arrangement of hemispheres by equating the center-to-center distance between neighboring particles, a, and the quantity $2r_d + 2r_o$. For a

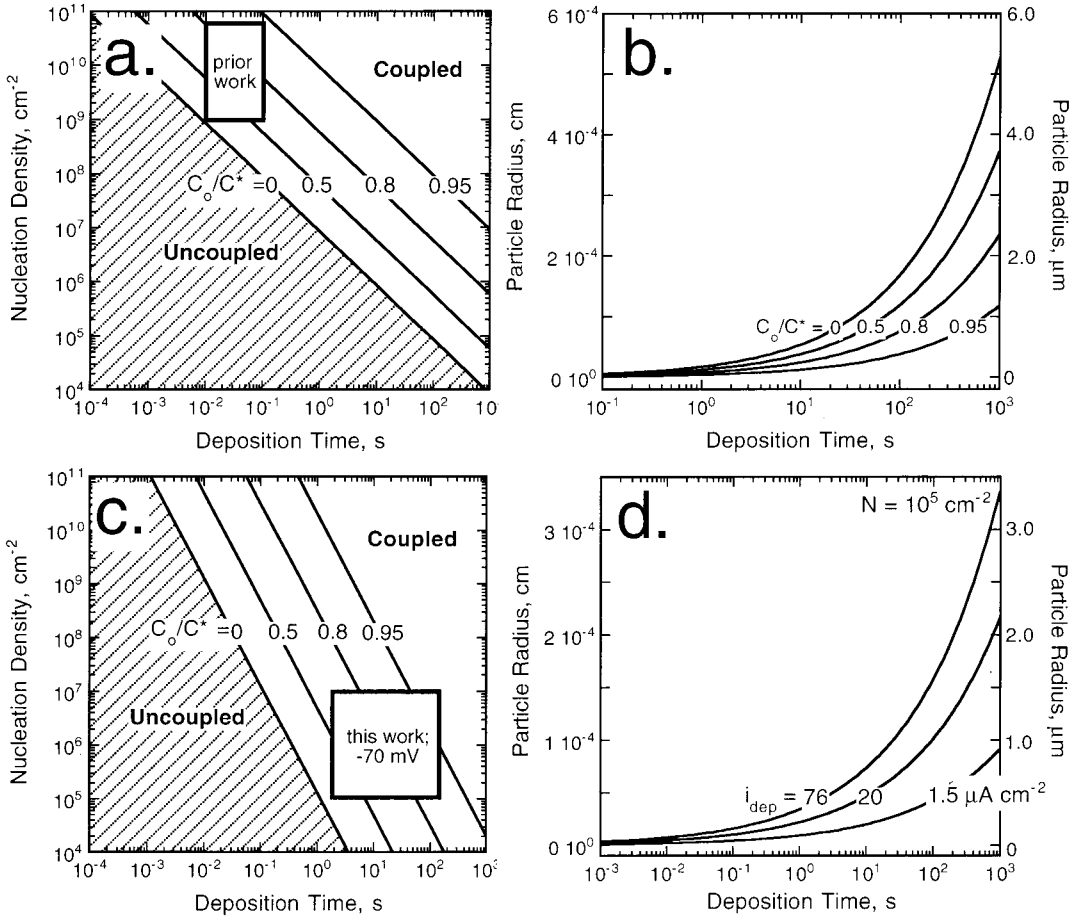

Figure 2. (a) t_c versus the nucleation density, N, calculated using eq 5, which is appropriate particle growth at diffusion control. This calculation is shown for several values of the dimensionless surface concentration of metal, C_o/C^*, as indicated. (b) r_o versus deposition time, using eq 3, for specified values of C_o/C^* as indicated. It is assumed that silver particles are deposited from a solution having $C^* = 1.0$ mM. (c) t_c versus the nucleation density, N, calculated using eq 6, which is appropriate particle growth at constant total current. This calculation is shown for several values of the dimensionless surface concentration of metal, C_o/C^*, as indicated. (d) r_o versus deposition time, using eq 4, for three values of the total deposition current, i_{dep}, as indicated. It is assumed that silver particles are deposited at a nucleation density of $N = 10^5$ cm^{-2}.

hexagonal array of particles, for example, diffusion-controlled growth (eq 3) yields

$$t_c = \frac{\rho}{\sqrt{3}NDC^*(1 - C_o/C^*)M[2 + 20(1 - C_o/C^*)]^2} \quad (5)$$

where N, the areal density of hemispheres on the surface, is given by $N = 2/(\sqrt{3}a^2)$. Growth at constant i_{dep} yields

$$t_c = \frac{0.8272z\pi F\rho}{i_{dep}MN^{1/2}[2 + 20(1 - C_o/C^*)]^3} \quad (6)$$

For randomly nucleated particles, the mean nearest-neighbor distance, $\langle a \rangle$, is related to the nucleation density through the same expressions.[16] Provided that the growth law for metal particles is in accordance with either eq 3 or eq 4, eq 5 or 6 provides a guide to the uncoupled electrodeposition of metal particles of any type, on any type of surface, subject to the constraint that nucleation is instantaneous.

Figure 2a shows how t_c is related to N and t_{dep} for a particular silver ion concentration of $C^* = 10^{-6}$ mol cm^{-3} (i.e., 1.0 mM), and for diffusion-controlled growth rates that are characterized by $C_o/C^* = 0.5$, 0.8, and 0.95. Notice that t_c increases by a factor of $\sim 10^3$ as C_o/C^* increases from 0 to 0.95. This means that the "retraction" of the depletion layer brought about by a reduced reaction rate can increase t_c very significantly. As shown in Figure 2b, the ability to deposit "large" metal particles is not compromised at reduced growth rates since the concomitant extension in t_c more than compensates. In fact, larger metal particles are accessible within the confines of the uncoupled regime. At a nucleation density of 10^7 cm^{-2}, for example, silver particles 2.0 μm in diameter can be prepared using a reduced growth rate which yields $C_o/C^* = 0.95$ ($t_c \approx 1000$ s), whereas the largest particles accessible at diffusion control ($t_c \approx 1$ s) are just 680 nm in diameter. For growth under conditions of constant i_{dep}, the relationship among t_c, N, and t_{dep} is as shown in Figure 2c, and a radius vs t_{dep} plot, appropriate for $N = 10^5$ cm^{-2}, is shown in Figure 2d. It is important to appreciate that, under conditions of constant total current, the surface concentration of metal ion, C_o, will increase as a function of deposition time (because the area of the metal particles continuously increases) provided i_{dep} does not exceed the diffusion-controlled rate. Thus, the contours of constant C_o/C^* shown in Figure 2c only serve to show qualitatively the effect of growth at reduced rates. Naturally, whether the growth law is eq 3 or 4 (or conceivably something else), the maximum diameter of the metal particles that may be obtained in an uncoupled electrodeposition experiment is inversely related to the nucleation density.

The area of N vs t_{dep} space sampled in our previous experiments[4,5]—conducted under conditions of diffusion control—is indicated by the region marked "prior work" in Figure 2a. This region lies completely within the boundaries of the coupled growth domain for $C_o = 0$, which is consistent with a variety

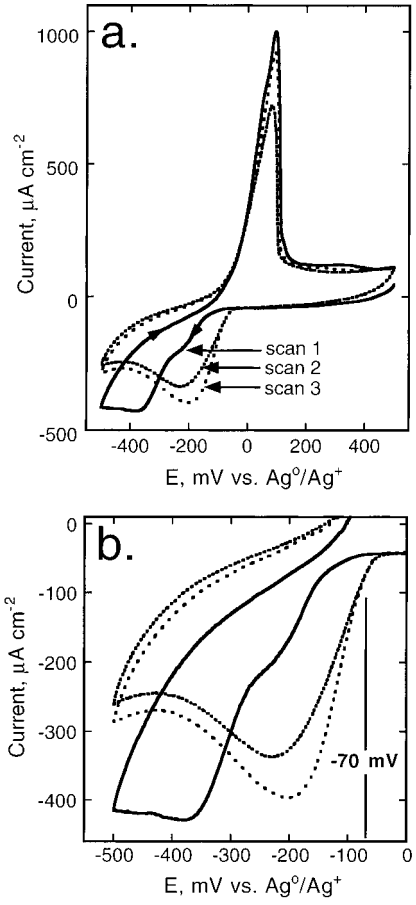

Figure 3. (a) Cyclic voltammograms at 20 mV s^{-1} for an HOPG electrode immersed in a silver-plating solution consisting of 1.0 mM $AgClO_4$ and 0.1 M $LiClO_4$ in acetonitrile. (b) Detail of (a) showing the onset of silver deposition.

of indications that interparticle coupling was present in those experiments. Figure 2 permits the conditions of N and t_{dep}, leading to uncoupled growth being readily identified, and particle electrodeposition experiments have not previously been conducted within this regime. We describe the first such experiments next.

III.B. Growth of Mesoscale Silver and Gold Particles in the Uncoupled Limit. Silver was selected for the initial study of uncoupled electrodeposition because the reduction of Ag^+ exhibits fast heterogeneous electron-transfer kinetics,[27] and because we have previously studied the growth of silver nanoparticles at large overpotentials on HOPG surfaces.[5] Cyclic voltammograms for a dilute silver-plating solution at an HOPG electrode are shown in Figure 3a. A nucleation overpotential of −100 mV is seen on the first negative-going voltammetric scan, but on subsequent scans, this overpotential is reduced to ∼−50 mV. We have recently demonstrated that the reduced overpotential for silver deposition on the second and subsequent scans is caused by the persistence on the HOPG surface of sub-1.0 nm silver clusters.[28] In Figure 3b, the silver plating waves are shown in greater detail. Here it can be seen that the deposition potential of −70 mV vs Ag^+/Ag^0 employed for many of the experiments described here is at the foot of the silver-plating wave for scans 2, 3, etc.

Current versus time transients for the electrodeposition onto HOPG are shown for several overpotentials in Figure 4a. In each experiment, a −500 mV × 5 ms "prepulse" was applied to induce nucleation prior to the application of a second, much longer pulse having the lower amplitude of −70 mV indicated

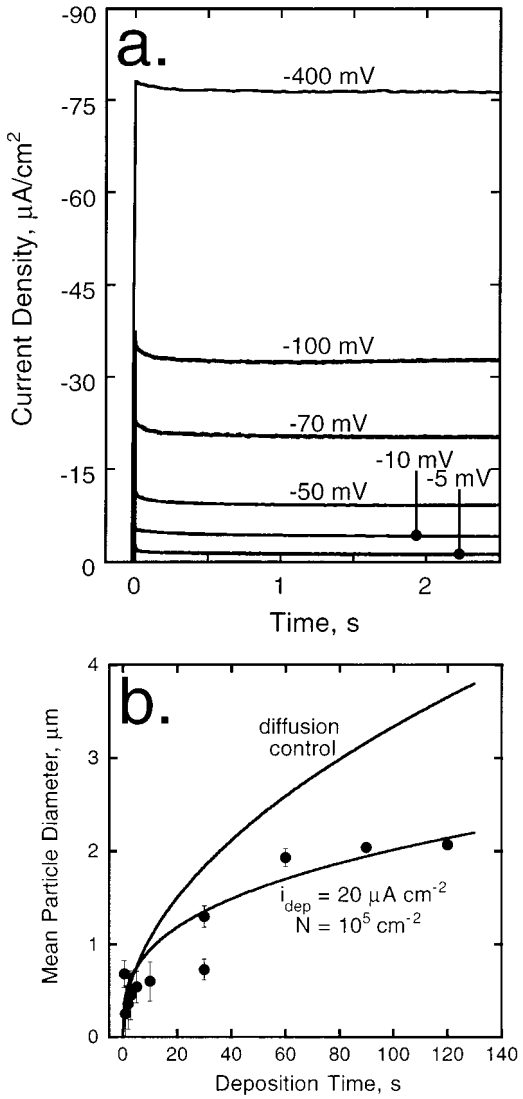

Figure 4. (a) Current versus time transients for the electrodeposition of silver on HOPG at specified plating potentials as shown. (b) Mean particle diameter, measured by SEM, versus electrodeposition time for experiments conducted at −70 mV vs Ag^+/Ag^0. Solid lines are the predicted diameter versus time for specified values of C_o/C^* using eq 3.

in Figure 3b. Only the current response to this second pulse is shown in Figure 4a. At all deposition potentials from −5 to −400 mV, silver deposition currents were observed to be virtually independent of time. This observation suggests that, within this potential range, electrodeposition is occurring under mixed kinetic and convective transport control. Since all experiments were carried out in quiescent plating solutions, the source of convection is the inevitable thermal motion of the electrolyte augmented, perhaps, by density gradients at the electrode surface caused by the depletion of silver ion. If the currents measured at −400 mV define the mass-transport-controlled limit (at even more negative potentials, background processes contributed to the measured current), then a rough estimate of C_{o,Ag^+} can be obtained for experiments carried out at −70 mV using the expression $I = nFAm_o(C^* - C_o)$, where m_o is the mass-transfer coefficient and A is the electrode area. This calculation yields a value for C_{o,Ag^+} of approximately 0.70 mM. This estimate permits the conclusion that the electrodeposition rate is well below the diffusion-controlled limit.

Since the deposition current is approximately constant, the particle radius should increase in proportion to $t^{1/3}$ according

to eq 4. In Figure 4b is plotted the mean particle diameter (from SEM measurements) as a function of the deposition time at −70 mV. The rate of growth is clearly lower than diffusion control (calculated using eq 3 with $C_o = 0$), and is approximately in accordance with eq 4 using $i_{dep} = 20\ \mu A\ cm^{-2}$ (as per the data of Figure 4a) and $N = 10^5\ cm^{-2}$. Experimentally measured nucleation densities ranged from 10^5 to $10^7\ cm^{-2}$ (vide infra).

On the basis of this information, parts c and d of Figure 2 make the following predictions: At a deposition potential of −400 mV, t_c ranges from 100 ms ($N = 10^7\ cm^{-2}$) to 1.0 s ($N = 10^5\ cm^{-2}$) corresponding to r_o values of 35 and 350 nm, respectively. We would expect the size dispersion of particles larger than these limits to be increased by interparticle diffusional coupling. At a deposition potential of −70 mV, it is likely that C_o/C^* is in the range from 0.5 to 0.7 with the result that t_c is increased by a factor of 10−100 across the range of nucleation densities. If the increase is a factor of 10, for example, then the attainable r_o values are 220−470 nm, respectively.

Let us first examine the characteristics of silver particles prepared using overpotentials of −400 and −500 mV and a deposition time of 150 ms. As we have already reported, the size dispersion of metal nanoparticles (Ag[5,6] and Pt[4]) prepared at these large overpotentials degrades rapidly as the t_{dep} exceeds 50 ms (corresponding to a mean diameter of ∼5 nm in these experiments). Typical SEM images of a surface prepared at −400 mV are shown in Figure 5a, while a typical surface prepared at −500 mV is shown in Figure 5b. On both surfaces, silver particles possess a mean diameter of ∼500 nm and are present at a nucleation density of $(2-5) \times 10^7\ cm^{-2}$. The similarity of the particle diameter on these two surfaces suggests that, at both −400 and −500 mV, particle growth occurred under conditions of diffusion control. The silver particles seen in Figure 5 exhibit substantial variation in size, and the particle diameter distributions for both samples are characterized by a RSD_{dia} of more than 30%. An examination of these SEM images reveals that the variations in diameter correlate with the local nucleation density on the surface: in both images, silver particles located in regions of locally high nucleation density ($N > 10^8\ cm^{-2}$) are small relative to particles that are located in sparsely nucleated regions of the surface ($N < 10^7\ cm^{-2}$), direct evidence that the growth of these particles occurred under the influence of interparticle diffusional coupling. These observations are consistent with the predictions of Figure 2a: on the basis of the mean value for N of $(2-5) \times 10^7\ cm^{-2}$, Figure 2a predicts a t_c in the range from 200 to 300 ms in these experiments. However, in densely nucleated regions of these surfaces where N is $10^8\ cm^{-2}$ or higher, t_c is <100 ms, and since the total deposition time was 150 ms in Figure 5, the particle growth rate in these high N regions should be depressed by interparticle diffusional coupling, exactly as seen in the SEM images of Figure 5.

The main focus of the experimental portion of this paper is the properties of silver particles prepared at a lower deposition potential of −70 mV vs Ag^+/Ag^0. In these experiments, a −500 mV × 5 ms pulse was first applied to nucleate silver particles, after which the deposition potential was reduced to −70 mV for the duration of the particle growth experiment (up to 120 s). As shown in Figure 3b scan 1, at −70 mV no silver deposition current is observed at a freshly cleaved graphite surface. This means that silver nuclei are not formed on clean graphite surfaces at this potential and the formation of new silver nuclei will cease upon the reduction of the plating potential from −500 mV (after 5 ms) to −70 mV. Thus, nucleation is temporally confined to the first 5 ms of growth, and instantaneous nucleation is assured. SEM images of silver particles prepared using deposition durations ranging from 500 ms to 120 s are shown in Figure 6. A comparison of the particles seen in these images with those deposited at −400 to −500 mV (Figure 6) reveals two major differences: First, silver particles grown at −70 mV are more narrowly dispersed in diameter. This is apparent from an examination of the particle size histograms (for the same samples imaged in Figure 6) which are shown in Figure 7. For the largest particles prepared at −70 mV (⟨dia⟩ > 0.75 μm), RSD_{dia} values below 8% were consistently obtained. Second, the nucleation density of 10^5 to $10^7\ cm^{-2}$ is 1−3 orders of magnitude lower.

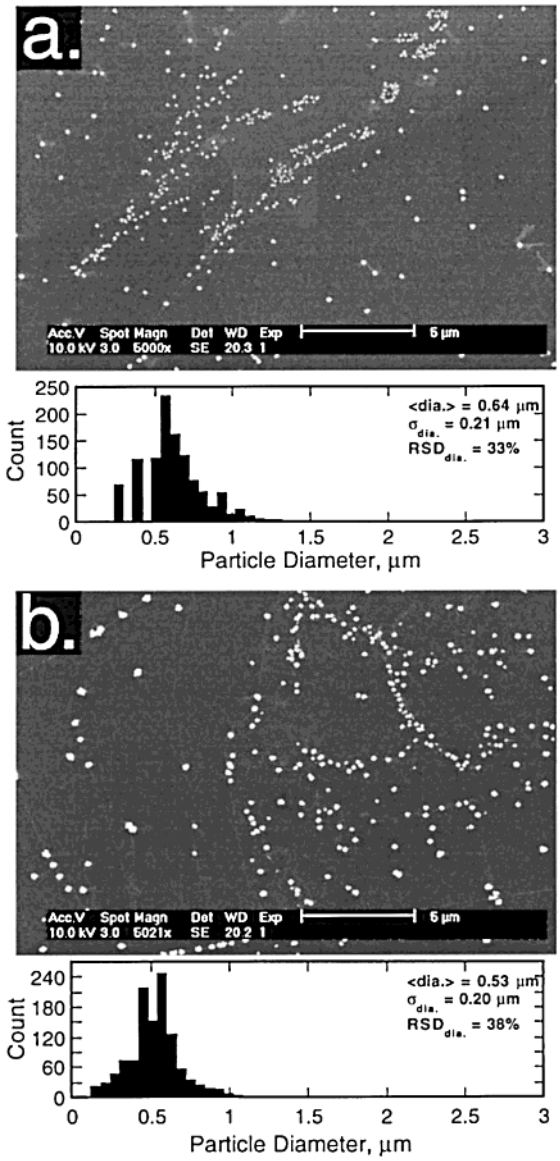

Figure 5. Scanning electron micrographs and particle size histograms for silver particles prepared using deposition potentials of −400 mV (a) and −500 mV (b) and a deposition duration of 150 ms.

The smallest particles analyzed in Figures 6 and 7 were 240 nm in diameter, but distributions of much smaller silver particles—from 100 to 42 nm in diameter—were obtained using shorter deposition durations down to 50 ms. The size monodispersity of these nanoscale particles was also very good (RSD_{dia} < 30%), but a rigorous statistical analysis involving hundreds of particles was precluded by the fact that just one particle could be observed in a single SEM or AFM image at the required magnifications.

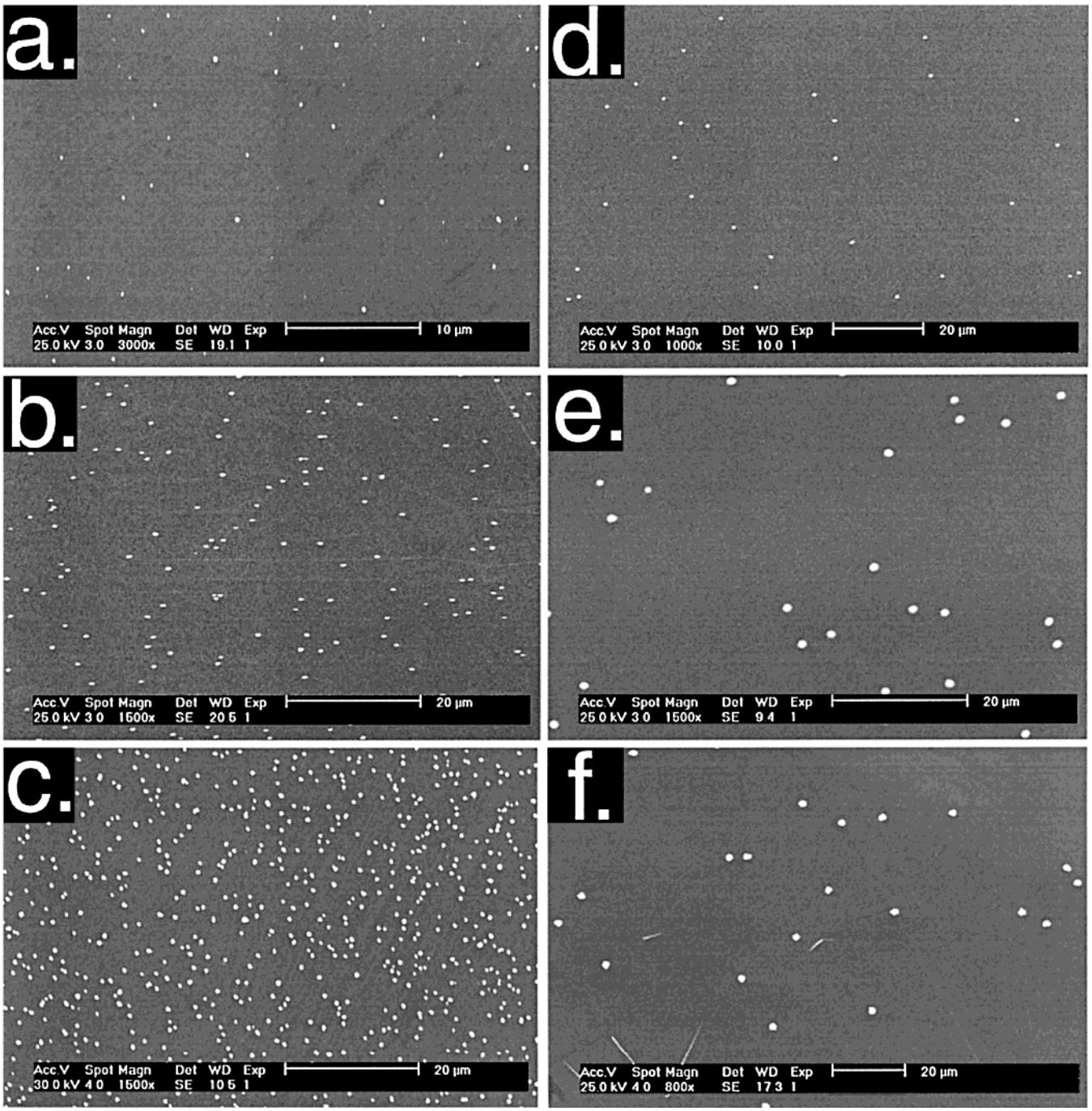

Figure 6. Scanning electron micrographs of silver particles prepared using a deposition potential of −70 mV and deposition durations of (a) 500 ms, (b) 1.0 s, (c) 5.0 s, (d) 10 s, (e) 30 s, and (f) 120 s.

Gold particles exhibiting a similar degree of size monodispersity were also obtained from aqueous, 1.0 mM $AuCl_3$ solutions. A representative SEM image of 0.8 μm diameter gold particles are shown in Figure 8a. One characteristic common to both gold and silver (Figure 8b) was the highly faceted appearance of particles prepared at low deposition potentials. This faceting suggests that the particles generated at low deposition potentials are single crystals.

In view of the fact that both −70 mV samples and the samples prepared at −400 to −500 mV are nucleated at −500 mV, the origin of the lower nucleation densities obtained −70 mV is unclear. What we *do* know regarding the nucleation of silver on these HOPG surfaces is the following: First, it is clear that, for $C^* = 10^{-6}$ mol cm^{-3}, the effect of a −500 mV bias pulse is to generate ∼1.0 nm diameter silver clusters at a coverage of 10^9 to 10^{10} cm^{-2} on the graphite surface. The fraction of these silver nanoparticles that mature into silver particles larger than 10 nm in diameter depends on the growth potential that is applied following the formation of these silver clusters. Even at the largest growth potentials we have explored of −500 mV, just 1 in 10 of the 1.0 nm clusters deposited initially matures into a silver particle having dimensions of 10 nm or more.[5] A silver particle attaining a diameter of 10 nm is certain to continue growing as we observe no systematic variation of the areal density of large particles (dia ≥ 10 nm) on the surface as a function of the deposition time. The probability of survival is much smaller—just 1 in 1000 on average—for particles grown at −70 mV. This variation in the probability for undergoing growth is an interesting and unexpected experimental observation that is worthy of further study, but we do not consider it

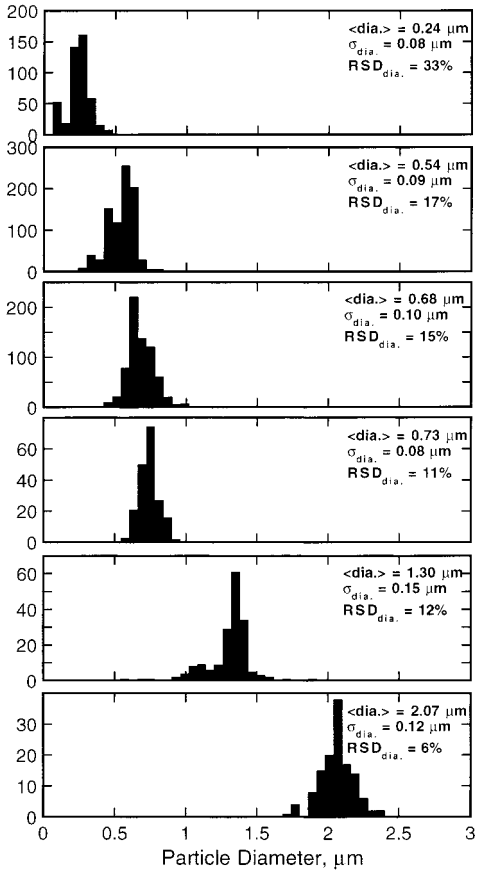

Figure 7. Particle size histograms and statistics for the same samples analyzed in Figure 6.

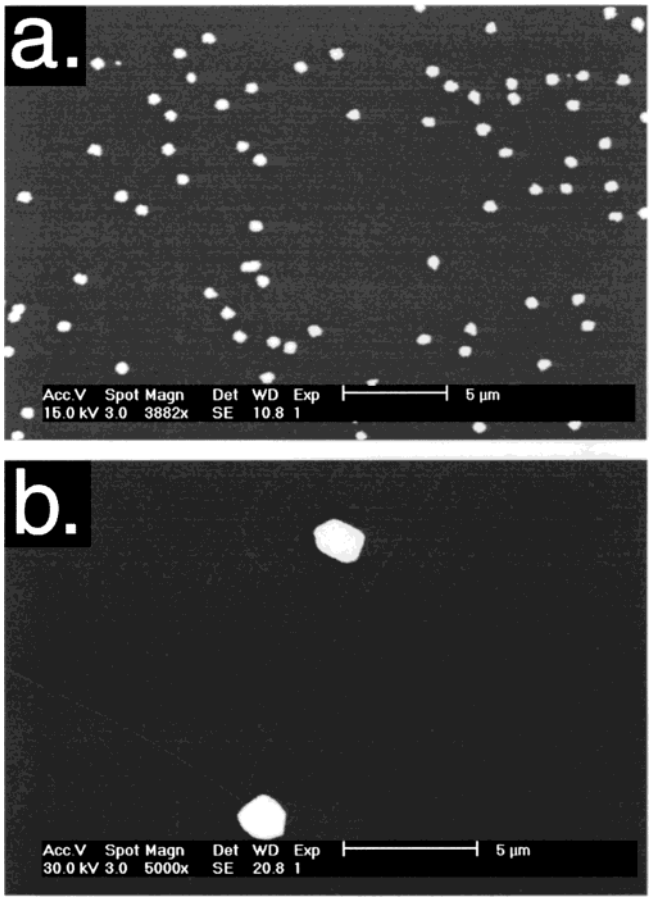

Figure 8. (a) Gold particles with a diameter of 1.0 μm grown for 2 s at 0.55 V vs SCE. (b) High-magnification SEM images of ~2.0 μm diameter silver particles showing faceting.

further here. It is important to note, however, that silver clusters that do not mature into larger particles also do not persist on the surface (AFM images, for example, show that nanometer-scale silver particles are absent from these surfaces following the growth of larger silver particles). Although the mechanism by which these nanoscopic particles disappear is also not understood, the coupled dissolution of these particles and concurrent deposition of silver onto larger particles (i.e., Ostwald ripening) is known to be a thermodynamically favorable process. A hypothesis has recently been advanced by Plieth and co-workers[29] which may account for a similar phenomenon observed for silver particle growth on the surface of indium tin oxide electrode surfaces.

Silver particles grown at −70 mV vs Ag^+/Ag^0 exhibit better size monodispersity than those grown at higher deposition potentials because of the absence of diffusional coupling at this potential. This conclusion is supported by two independent observations. In Figure 9a, the standard deviation of the particle diameter, σ_{dia}, and the RSD_{dia} are both plotted as a function of the particle areal density on the surface. Brownian dynamics simulations of silver particle growth have demonstrated that for particles of a particular diameter, σ_{dia} increases with increasing nucleation density. No evidence for such a correlation is seen in the data plotted in Figure 9a.

Further confirmation that diffusional coupling is not occurring at −70 mV is provided by the data plotted in Figure 9b. At the top of Figure 9b are shown two "correlation plots" of the mean diameter of two nearest neighbors as a function of the interparticle distance. In these plots, a positive slope indicates that the mean diameter of two nearest neighbors increases with the distance separating them. This is the expected result if interparticle diffusional coupling is operating during growth. Both the slopes and the correlation coefficients for these plots were reproducibly greater for samples prepared at −500 mV. This is shown in Figure 9b, where—for 11 samples prepared at either −500 or −70 mV—the slopes of the correlation plots have been plotted versus the *R* values obtained from the linear regression analysis.[30] For samples prepared at −70 mV, a *negative* slope—indicating an inverse correlation of the particle diameter with the interparticle spacing—was seen in two of six experiments (Figure 10). This analysis suggests that interparticle diffusional coupling is present in electrodeposition experiments conducted at −500 mV, but is absent, or nearly so, in the experiments conducted at −70 mV.

IV. Summary

The main conclusions of this paper are the following.

(a) The radius of the depletion layer surrounding each metal particle, r_d, is proportional to the quantity $C^* - C_o$. Consequently, the growth of metal particles from small concentrations of metal ion, C^*, and/or at reduced reaction rates (resulting in nonzero C_o) forestalls interparticle diffusional coupling, increases t_c, and permits the growth of larger particles prior to the onset of diffusional coupling. The utility of "slow growth" for achieving narrow particle size distributions is the most important conclusion of this paper.

(b) For the growth of mesoscale silver and gold particles on graphite, we have found that conditions of nucleation density and reaction rate within the uncoupled parameter space are experimentally accessible. In this study, uncoupled growth was achieved using nucleation densities in the range from 10^5 to 10^7 cm^{-2} and a deposition overpotential of −70 mV. Under

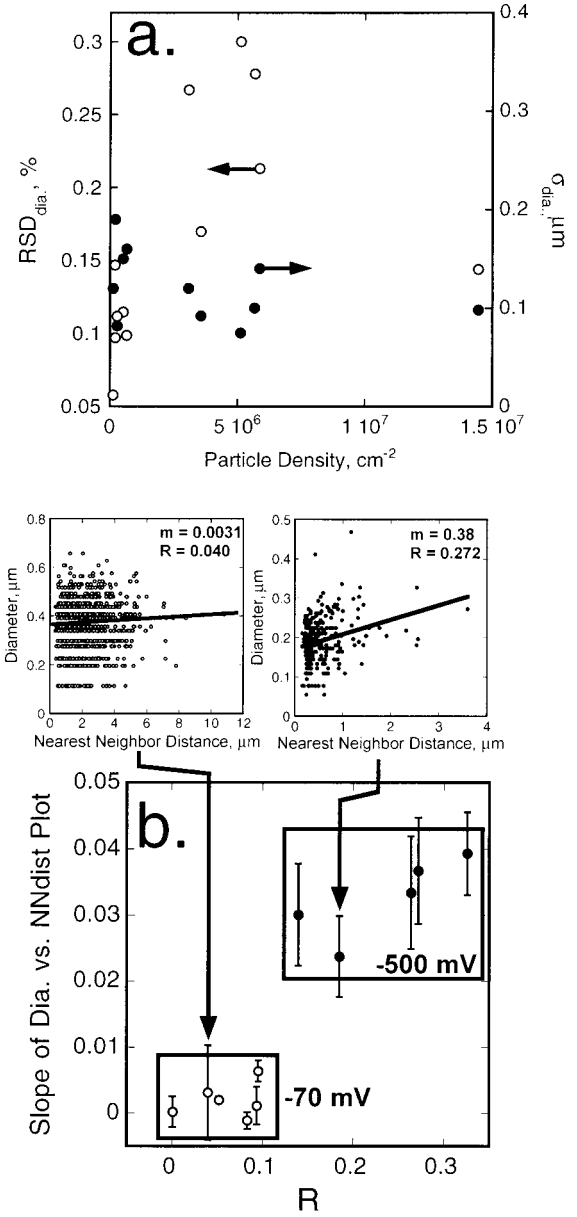

Figure 9. (a) Relative standard deviation of the mean particle diameter (○) and the standard deviation of the particle diameter (●) versus the particle areal density for experiments conducted at −70 mV vs Ag^+/Ag^0. (b) (Top) Typical mean diameter vs interparticle separation distance "correlation plots" for neighboring silver particles on the graphite surface. The plot at top left (○) is for a sample prepared at −70 mV, and that at top right (●) at −500 mV. (Bottom) Slope of the correlation plot versus *R*, the correlation coefficient, for experiments conducted at −70 mV vs Ag^+/Ag^0 (○) and at −500 mV (●). The error bars represent ±1 standard deviation of the slope values from the regression line.

these conditions, silver and gold particle distributions exhibiting RSD_{dia} values below 10% were obtainable.

(c) For experiments carried out at −500 mV, a clear correlation exists between the distance between neighboring particles and the mean size of two nearest neighbors. This "fingerprint" of interparticle diffusional coupling is not seen for silver particle dispersions prepared at −70 mV. This result provides support for the hypothesis that interparticle diffusional coupling provides the primary mechanism by which size dispersion develops in metal particles prepared by electrodeposition.

There is still room for improvement. In particular, we have so far been unable to generate metal particle under conditions

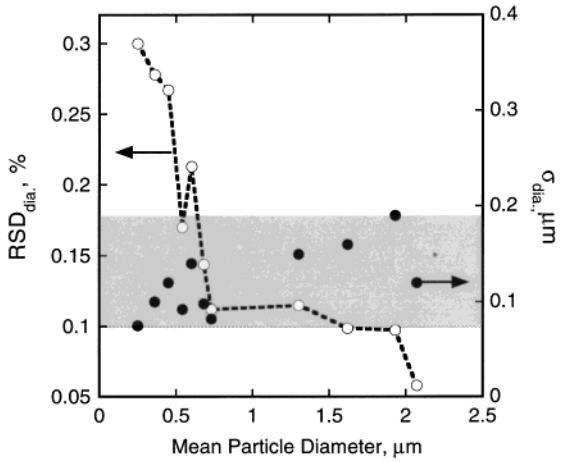

Figure 10. σ_{dia} and RSD_{dia} versus deposition time for the data of Figure 9a pertaining to the growth at −70 mV of silver particles.

leading to the narrowing of particle size distributions as a function of deposition time. As shown in Figure 7, the σ_{dia} values are virtually invariant with t_{dep}. This is not the expected outcome for the growth law of eq 4, which predicts $dr/dt \propto t^{-2/3}$, implying dr/dt is larger for smaller particles. Instead, distribution narrowing is predicted. Our inability to observe distribution narrowing means one of two things: A second and as yet unidentified mechanism of distribution broadening—in addition to diffusional interparticle coupling—is operating in these experiments. Alternatively (or in addition), there is the possibility that some residual level of diffusional coupling is still present but undetected in our experiments. A more rigorous test of eqs 5 and 6 will require a system which enables the nucleation density to be tuned over much larger ranges independent of the reaction rate.

Acknowledgment. This work was funded by the National Science Foundation (Grant DMR-9876479) and the donors of the Petroleum Research Fund of the American Chemical Society (Grant 33751-AC5). We also gratefully acknowledge the financial support of the A.P. Sloan Foundation Fellowship, and the Camille and Henry Dreyfus Foundation.

References and Notes

(1) Throughout this paper, the terms "dimensional uniformity" and "size monodispersity" applied to the particle diameter refer to the proximity of the relative standard deviation of the particle diameter (RSD_{dia}, the ratio of the mean diameter to the standard deviation of the diameter) to zero.

(2) "Mesoscale" will refer to a critical dimension in the range from 10 Å to 100 μm.

(3) The first exception involves recent work from Plieth and co-workers (Plieth, W.; Dietz, H.; Sandmann, G.; Meixner, A.; Weber, M.; Moyer, P.; Schmidt, J. *Electrochim. Acta* **1999**, *44*, 3659.), who have described the preparation of ∼100 nm diameter silver particles exhibiting excellent size monodispersity. In those experiments, silver particles were deposited under conditions which—as demonstrated in this paper—are expected to yield uncoupled growth. The second involves the growth by Zach and Penner (Zach, M. P.; Penner, R. M. *Adv. Mater.* **2000**, *12*, 878) by "H_2-coevolution" of mesoscale nickel particles.

(4) Zoval, J. V.; Lee, J.; Gorer, S.; Penner, R. M. *J. Phys. Chem.* **1998**, *102*, 1166.

(5) Zoval, J. V.; Stiger, R. M.; Biernacki, P. R.; Penner, R. M. *J. Phys. Chem.* **1996**, *100*, 837.

(6) Stiger, R.; Craft, B.; Penner, R. M. *Langmuir* **1999**, *15*, 790.

(7) Foss, C. A.; Tierney, M. J.; Martin, C. R. *J. Phys. Chem.* **1992**, *96*, 9001.

(8) Foss, C. A.; Hornyak, G. L.; Stockert, J. A.; Martin, C. R. *J. Phys. Chem.* **1994**, *98*, 2963.

(9) Preston, C. K.; Moskovits, M. *J. Phys. Chem.* **1993**, *97*, 8495.

(10) Sun, L.; Searson, P. C.; Chien, C. L. *Appl. Phys. Lett.* **1999**, *74*, 2803.

(11) Whitney, T. M.; Jiang, J. S.; Searson, P. C.; Chien, C. L. *Science* **1993**, *261*, 1316.
(12) Searson, P. C.; Cammarata, R. C.; Chien, C. L. *J. Electron. Mater.* **1995**, *24*, 955.
(13) Bäumer, M.; Frank, M.; Libuda, J.; Stempel, S.; Freund, H.-J. *Surf. Sci.* **1997**, *391*, 204.
(14) Klimenkov, M.; Nepijko, S.; Kuhlenbeck, H.; Bäumer, M.; Schlögl, R.; Freund, H.-J. *Surf. Sci.* **1997**, *391*, 27.
(15) Röder, H.; Hahn, E.; Brune, H.; Bucher, J.-P.; Kern, K. *Nature* **1993**, *366*, 141.
(16) Fransaer, J.; Penner, R. M. *J. Phys. Chem. B* **1999**, *103*, 7643.
(17) LaMer, V. K.; Dinegar, R. H. *J. Am. Chem. Soc.* **1950**, *72*, 4847.
(18) Reiss, H. *J. Chem. Phys.* **1954**, *19*, 482.
(19) Sugimoto, T. *Adv. Colloid Interface Sci.* **1987**, *28*, 65.
(20) Overbeek, J. T. G. *Adv. Colloid Interface Sci.* **1982**, *15*, 251.
(21) Tong, W. M.; Williams, R. S. *Annu. Rev. Phys. Chem.* **1994**, *45*, 401.
(22) Tong, W. M.; Williams, R. S.; Yanase, A.; Segawa, Y.; Anderson, M. S. *Phys. Rev. Lett.* **1994**, *72*, 3374.
(23) Ngo, T. T.; Williams, R. S. *Appl. Phys. Lett.* **1995**, *66*, 1906.
(24) Crank, J. *The Mathematics of Diffusion*, 2nd ed.; Oxford Unversity Press: New York, 1975.
(25) Scharifker, B. R. *J. Electroanal. Chem.* **1999**, *458*, 253.
(26) Gunawardena, G.; Hills, G.; Montenegro, I. *J. Electroanal. Chem.* **1982**, *138*, 241.
(27) Porter, J. D.; Robinson, T. O. *J. Phys. Chem.* **1993**, *97*, 6696.
(28) Ng, K.; Liu, H.; Penner, R. M. *Langmuir* **2000**, *16*, 4016.
(29) Sandmann, G.; Dietz, H.; Pleith, W. *J. Electroanal. Chem.*, in press.
(30) *R* is the square root of the coefficient of determination, often used to express the degree to which a regression line predicts the actual *Y* vs *X* data. A formal definition of *R* is

$$R = S_{XY}/(S_X S_Y)^{1/2}$$

where $S_{XY} = \sum(X - \langle X\rangle)(Y - \langle Y\rangle)$, $S_X = \sum(X - \langle X\rangle)^2$, and $S_Y = \sum(Y - \langle Y\rangle)^2$. See, for example: Sachs, L. *Applied statistics: A Handbook of Techniques*, 2nd ed.; Reynarowych, Z., Trans.; Springer-Verlag: New York; Academic Press: New York, 1984.